

Longitudinal electron bunch diagnostics using coherent transition radiation

D. Mihalcea,¹ C. L. Bohn,¹ U. Happek,² and P. Piot^{1,3}

¹*Northern Illinois University, DeKalb, Illinois 60115, USA*

²*University of Georgia, Athens, Georgia 30602, USA*

³*Fermilab, Batavia, Illinois 60510-0500, USA*

(Received 20 March 2006; published 17 August 2006)

The longitudinal charge distribution of electron bunches in the Fermilab/NICADD photoinjector was determined using the coherent transition radiation produced by electrons passing through a thin metallic foil. The autocorrelation of the transition radiation signal was measured with a Michelson-type interferometer. The response function of the interferometer was determined from measured and simulated intensity spectra for low electron bunch charge and maximum longitudinal compression. Both pyroelectric and Golay detectors were used for these measurements. A Kramers-Kronig technique was used to determine longitudinal charge distribution. Measurements were performed for electron bunch lengths in the range from 0.3 to 2 ps (rms). To test the accuracy of this interferometric method, the longitudinal charge distribution was measured for double-peaked electron bunches with known distance between the two pulses. The agreement between measured bunch length and simulation is within 30%.

DOI: [10.1103/PhysRevSTAB.9.082801](https://doi.org/10.1103/PhysRevSTAB.9.082801)

PACS numbers: 29.27.Fh, 41.60.-m

I. INTRODUCTION

Progress toward producing free electron lasers (FEL) in the x-ray domain is contingent on the quality of the electron beam which is passed through the periodic array of magnets. To achieve coherence of the FEL radiation, the electron bunch length must be in the subpicosecond range [1]. To avoid large beam emittance growth, it is convenient to compress the electron bunches after several acceleration stages when space charge forces decrease significantly. In many cases, such short bunches are obtained by compressing the beam in magnetic chicanes. As a result, the longitudinal charge distribution is significantly distorted from its original Gaussian shape. Therefore, to determine parameters like peak current, or FWHM, it is important to have a complete measurement of the bunch longitudinal charge distribution rather than just an estimate of its length. This kind of measurement is also important for longitudinal beam diagnostics at the future International Linear Collider where the bunch length at the interaction point will likely be in the picosecond range [2]. High-resolution measurement of complicated longitudinal charge density is the subject of this paper.

Coherent transition radiation (CTR) [3,4] can be produced by a bunch of charged particles when it crosses a metallic foil. The intensity of CTR can be related to the form factor of the charge distribution $f(\omega)$ [5,6]:

$$I(\omega) = N(N-1)I_e|f(\omega)|^2, \quad (1)$$

where N is the total number of electrons in the bunch and I_e is the radiation emitted by a single electron. In the limit of perfectly conducting metallic foil, I_e does not depend on frequency. For transversely focused relativistic beams moving in the z -direction (line charge approximation), the form factor $f(\omega)$ can be expressed in terms of the normal-

ized longitudinal charge distribution $\rho(z)$:

$$f(\omega) = \int \rho(z) \exp(i\omega z/c) dz. \quad (2)$$

Since only the intensity spectrum $I(\omega)$ can be experimentally measured, the phase of the form factor is unknown. However, the frequency-dependent phase of the form factor can be well approximated if $I(\omega)$ is known for the entire wavelength spectrum (Kramers-Kronig method [7]):

$$\psi(\omega) = -\frac{2\omega}{\pi} \int_0^\infty dx \frac{\ln[\kappa(x)/\kappa(\omega)]}{x^2 - \omega^2}, \quad (3)$$

where $\kappa(\omega) \equiv \sqrt{I(\omega)}$. With this approximation, the normalized longitudinal charge distribution is given by

$$\rho(z) = \frac{1}{\pi c} \int_0^\infty \kappa(\omega) \cos[\psi(\omega) - \omega z/c] d\omega. \quad (4)$$

Longitudinal profile measurements were performed at the Fermilab/NICADD Photoinjector Laboratory [8]. Typically, the electron energy is about 16 MeV and the root-mean-square (rms) bunch duration ranges from 2 to 10 ps when the bunch charge is a few nanocoulombs. Electron bunches are compressed in the subpicosecond range with a four-dipole magnetic chicane located downstream from the accelerating structures.

CTR was used by several other groups to measure the longitudinal charge density of electron bunches [9–12]. A major problem that all groups encountered is that the intensity of the coherent transition radiation [Eq. (1)] is strongly distorted by the measuring devices, over the whole frequency spectrum.

One approach partially to avoid this problem is to complete the intensity spectrum by making some reasonable assumptions about its shape at low and high frequencies

[9,10]. Another approach is to avoid the use of the Kramers-Kronig method (which requires the intensity for all frequencies) by assuming that bunches have a predefined shape (Gaussian or superposition of two Gaussians), parametrized by some free parameters. These free parameters can be extracted from the measured intensity spectra, also corrected to account for the depletion at low frequencies [11,12].

The approach we use here is different. First, we determine the transmission of the experimental device for a large frequency range. Then, this response function of the apparatus is used to correct the measured intensity spectra. There is no need to make any assumptions about the longitudinal shape of the electron bunches. We tested our method for complicated bunch shapes like double-peaked non-Gaussian pulses.

Section II of this paper contains a brief description of the Michelson interferometer and the definitions of the experimentally measured quantities. The interferometer (including the detectors) does not have a flat response over the frequency domain of interest; Sec. III describes how this problem is overcome. Section IV contains details about data processing. A brief summary and a few conclusions about this method can be found in Sec. V.

II. MICHELSON INTERFEROMETER

CTR is produced by electron bunches crossing an aluminum foil oriented 45° with respect to the beam line. Only the transition radiation emitted on the same side of the aluminum foil 90° of the incident electron beam is collected (backward radiation). Between the aluminum foil and the Michelson interferometer, shown schematically in Fig. 1, there are a single-crystal quartz window and two off-axis gold-coated parabolic mirrors which convert the divergent beam to a parallel one.

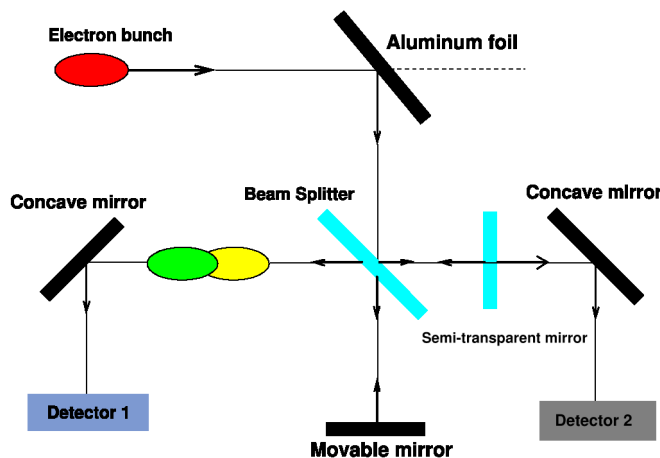


FIG. 1. (Color) Michelson interferometer. Detector 1 is used to record the autocorrelation function. Detector 2 is a reference detector used to normalize the autocorrelation function.

The beam splitter is coated with a thin inconel layer of thickness chosen such that transmission and reflection are 30% and independent of the wavelength up to the plasma frequency. One arm of the interferometer has a mirror mounted on a translation stage which motion can be remotely controlled. The right arm of the interferometer contains a semitransparent mirror which has constant 30% transmission and 30% reflection coefficients within the relevant wavelength range. Transmitted radiation is focused on the reference detector by an off-axis parabolic mirror. The combined radiation from the movable mirror and from the reflection on the semitransparent mirror is focused on the detector in the left arm of the interferometer.

The autocorrelation signal is the superposition of the time-dependent electric fields from the two arms of the interferometer, and it is recorded by the first detector as a function of the path difference δ :

$$I_1 \propto \int_{-\infty}^{+\infty} |E(t + \delta/c) + E(t)|^2 dt. \quad (5)$$

The intensity recorded by the second detector does not depend on path difference but senses fluctuations from beam jitters, as does the first detector. Therefore it is convenient to define the autocorrelation function $S(\delta)$ as the ratio of the intensities measured by the two detectors:

$$S(\delta) \equiv \frac{I_1}{I_2} \propto \frac{\text{Re} \int E(t)E^*(t + \delta/c) dt}{\int |E(t)|^2 dt}. \quad (6)$$

The intensity I_1 was measured with either a pyroelectric detector [13] or with a Golay cell [14]. The reference intensity I_2 was always measured with the less expensive pyroelectric detector. Equation (6) can be rewritten in frequency domain as

$$S(\delta) \propto \frac{\text{Re} \int |E(\omega)|^2 e^{-i\omega\delta/c} d\omega}{\int |E(\omega)|^2 d\omega}, \quad (7)$$

where $E(\omega)$ is the Fourier transform of $E(t)$. The intensity $I(\omega)$ can simply be obtained from the autocorrelation function $S(\delta)$ through an inverse Fourier transform:

$$I(\omega) \equiv |E(\omega)|^2 \propto \int_{-\infty}^{+\infty} S(\delta) e^{i\omega\delta/c} d\delta. \quad (8)$$

III. INTERFEROMETER RESPONSE FUNCTION

Transition radiation is emitted by each charged particle in the beam bunch when it crosses the boundary between two media with different indices of refraction. Coherence of the transition radiation is achieved when the phases of the waves emitted by individual particles are close each other. Coherence implies that the longitudinal size of the beam must be smaller than the wavelength of transition radiation. At the Fermilab/NICADD photoinjector, the typical bunch duration after compression is in the range

0.3 to 2 ps when the charge of the electron bunch varies from 0.5 nC to a few nanocoulombs, respectively. Therefore the interferometer must be sensitive at wavelengths in the millimeter range.

The biggest limitation for methods which use coherent transition radiation to characterize the longitudinal bunch profile comes from the nonuniform apparatus response with respect to radiation wavelength. Since the most valuable information carried by CTR is in its low-frequency component (below 1 THz), the interferometer’s sensitivity in this spectral region must be carefully investigated.

For our measurements we used pyroelectric detectors and Golay cells. Direct measurements of apparatus sensitivity in the far-infrared region are hard to perform and need expensive equipment. Therefore, we relied on indirect estimates based on simulations.

At the Fermilab/NICADD photoinjector, extensive efforts were dedicated to understanding and modeling the electron bunch compressor [15]. Parmela [16] and Impact-T [17] simulation codes were used to determine the longitudinal bunch profile for some given experimental conditions.

In order to determine the interferometer response function, both experimental and simulated intensity spectra must be determined. The experimental intensity $I_{\text{exp}}(\omega)$ is determined by Fourier transforming the measured autocorrelation function [Eq. (8)]. Figure 2 (top plots) displays the measured autocorrelation function and the intensity spectrum for 0.5 nC electron bunches at maximum compression when pyroelectric detectors were used. The simu-

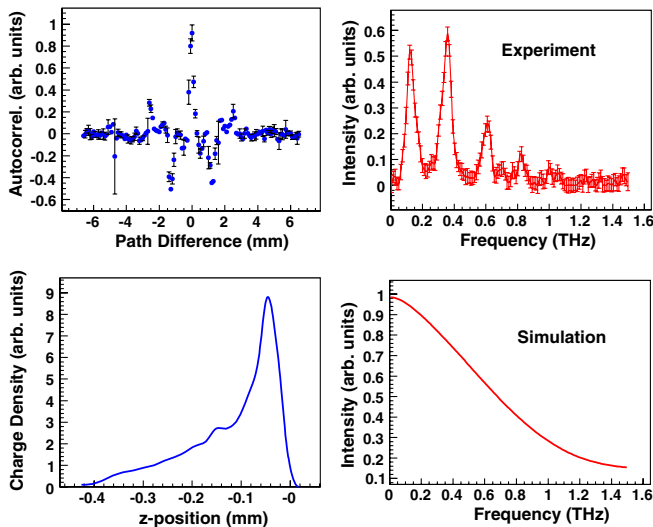


FIG. 2. (Color) Top plots: measured autocorrelation and intensity spectrum for 0.5 nC electron bunches at maximum compression. These measurements were performed with pyroelectric detectors following the procedure described in Sec. IV. Bottom plots: simulation results for longitudinal charge density and intensity spectrum also for 0.5 nC electron bunches at maximum compression.

lated intensity $I_{\text{sim}}(\omega)$ (Fig. 2 bottom right plot) is the Fourier transform of the longitudinal bunch profile obtained from simulations [Eq. (2)] (Fig. 2 bottom left plot). By definition the apparatus response function is

$$R(\omega) \equiv \frac{I_{\text{exp}}(\omega)}{I_{\text{sim}}(\omega)}. \tag{9}$$

The response function of the interferometer was determined for both pyroelectric and Golay detectors (Fig. 3). The intensities $I_{\text{exp}}(\omega)$ and $I_{\text{sim}}(\omega)$ from Eq. (9) were determined for 0.5 nC electron bunches at maximum compression.

The shape of the response function strongly depends on the type of detector which is used. The sensitive part of the pyroelectric detectors consists of a 100 μm thickness layer of LiTaO₃ crystal sandwiched by two thin (100 Å) chromium layers. Because of the interference on the backplane of the crystal, the response function of the detector (and also of the whole interferometer) has an amplitude modulation. This effect was also observed by other groups [18,19]. Direct experimental measurements of the pyroelectric detectors’ response function were performed at Brookhaven NSLS [20].

Simulation results for the response function were obtained from the ratio between the measured intensity spectrum and the simulated one [Eq. (9)] when 0.5 nC electron bunches are at maximum compression. Direct experimental measurements of the response function (for pyroelectric detectors only) and simulations for both pyroelectric and Golay detectors are shown in Fig. 3.

The diffraction effects on optical components contributes to lower values of the response function in the low-

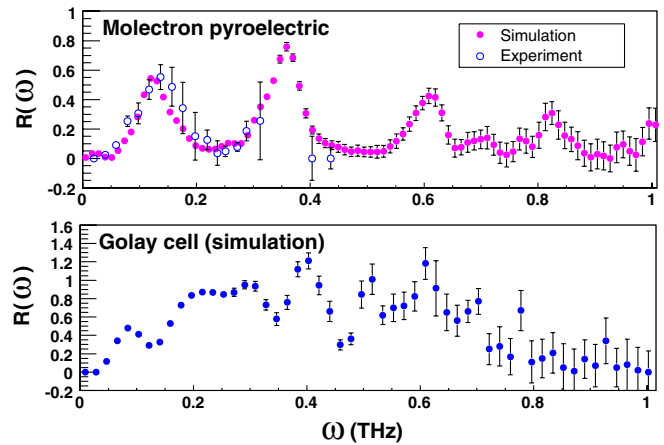


FIG. 3. (Color) Interferometer response functions. Top plot: response function of the interferometer with pyroelectric detectors from simulation (red bullets) and direct measurements (open circles). Bottom plot: response function of the interferometer equipped with a Golay detector from simulation. In both cases the simulation results were obtained from the division of the measured intensity spectrum and the simulated one when 0.5 nC electron bunches are at maximum compression.

frequency domain [21]. With typical values for beam energy (≈ 12 MeV) and detector size (6 mm), Eq. (14) from [21] gives about 0.05 THz where the intensity spectrum decreases 10% from its maximum value. In the case of the Golay detector the response function starts to significantly decrease from about 0.2 THz (Fig. 3). This means that lower detector sensitivity in the far-infrared domain, rather than diffraction, appears to be the major factor for the reduction of the response function at low frequencies.

In the case of pyroelectric detectors, diffraction and the already mentioned distortion of the response function due to interference are the main causes for diminished sensitivity at low frequencies. At high frequencies, for both types of detectors, the response function decreases slowly mainly due to absorptions in the quartz window located before the entrance to the interferometer.

The response function $R(\omega)$ is used to correct the intensity spectrum when measurements are performed under arbitrary experimental conditions. In addition to this correction, the intensity spectrum must also be completed for missing frequencies. This procedure will be explained in the following section.

IV. DATA ANALYSIS

A. Autocorrelation and intensity spectra

During a data-taking session, the position of the movable mirror is changed with a predefined step (typically $50 \mu\text{m}$). At each position of the movable mirror, the intensities I_1 and I_2 [Eq. (6)] are measured. Typically, five such measurements are performed and average values of I_1 and I_2 , as well as their standard deviations are recorded. The intensity of the UV laser varies from shot to shot and so does the electron bunch charge. These variations are up to 50% of the nominal laser intensity. Since the intensity of the coherent radiation depends on square of the electron bunch charge [Eq. (1)], the intensities I_1 and I_2 are measured only if the bunch charge is within some narrow limits, typically less than 10% away from the nominal charge. We built a numerical filter to restrict our measurements to bunch charges in this range.

The autocorrelation functions and intensity spectra (Fourier transforms of the autocorrelation functions) are shown in Figs. 4 and 5, respectively, for 0.5 nC electron bunches at maximum compression, when detectors are “ideal” (flat response function), pyroelectric, and Golay. The plots for the “ideal detector” in Figs. 4 and 5 are derived from the simulated bunch shape shown in Fig. 2 assuming that the response function is flat. Also, the plots for the Molelectron pyroelectric detectors are the same as those from Fig. 2.

The nonuniform interferometer response function has a big effect on both autocorrelation and intensity spectra. Because of the oscillatory shape of the response function when the interferometer is equipped with pyroelectric

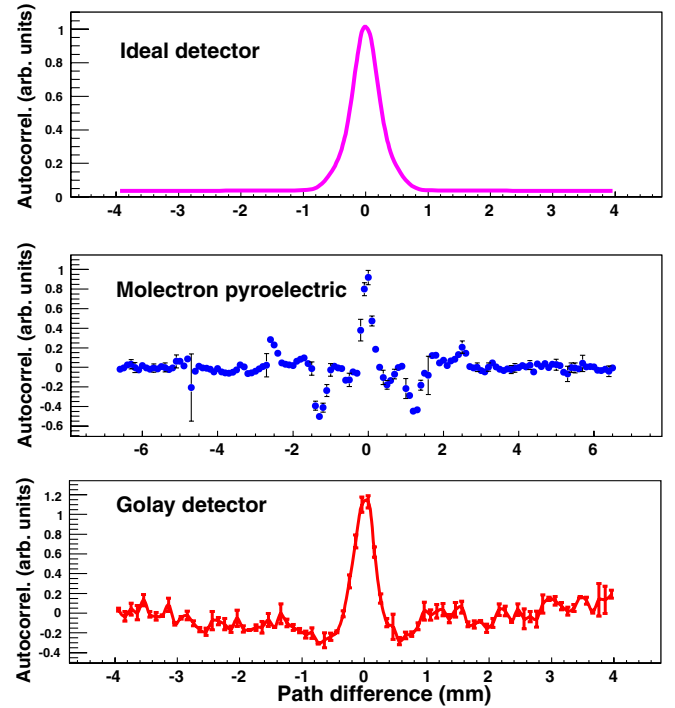


FIG. 4. (Color) Autocorrelation functions for ideal (top), pyroelectric (middle), and Golay (bottom) detectors. Experimental autocorrelation function for Molelectron pyroelectric detectors is the same as the one displayed in Fig. 2.

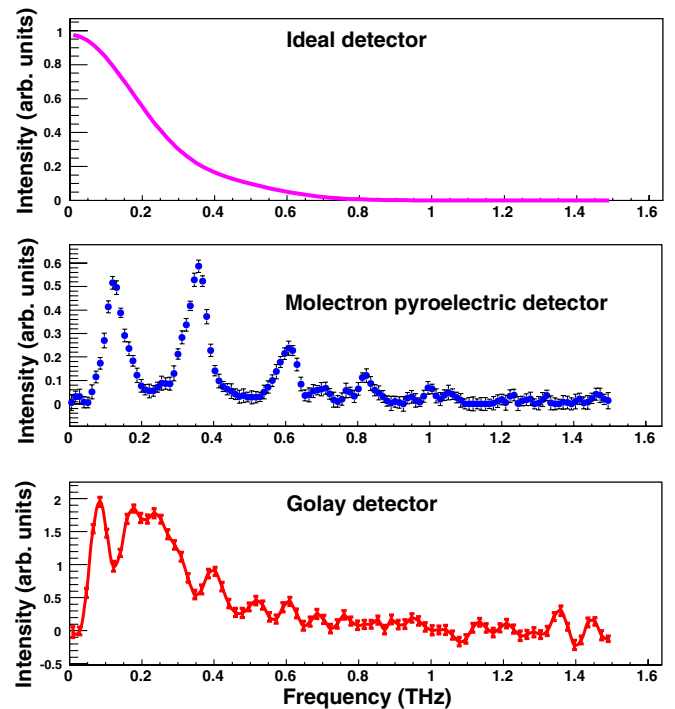


FIG. 5. (Color) Intensity spectra for ideal (top), pyroelectric (middle), and Golay (bottom) detectors. Vertical axis has arbitrary units.

detectors, the autocorrelation and intensity spectra are more distorted compared to the case of Golay detectors. Therefore, we decided to use a Golay detector for most of our measurements.

B. Intensity spectrum completion

The interferometer's response function is used to correct intensity spectra when electron bunches are produced under some arbitrary experimental conditions. Corrected intensity spectra still do not cover the whole spectral range. The reason is that the interferometer's response function is close to zero at low and high frequencies. Therefore, in order to apply the Kramers-Kronig method [Eq. (4)], the corrected intensity spectrum must also be completed for the missing frequencies. At low and high frequencies, intensity spectra were approximated with functions valid for the asymptotic regions (Ref. [7]):

$$I(\omega) \approx a + b\omega^2, \quad \omega \ll \omega_0, \quad (10)$$

$$I(\omega) \approx \alpha\omega^\beta, \quad \omega \gg \omega_0. \quad (11)$$

with $\omega_0 = c/\sigma_z$. The values of the unknown parameters a, b, α, β were determined by fitting the asymptotic expressions with the available data points.

Figure 6 shows an example of the spectrum-completion procedure for 3.2 nC electron bunches at moderate compression. Since the compression in this case is only moderate, the electron bunches are longer, and consequently the coherent component of the transition radiation is even farther in the infrared region where the instrument is less sensitive. Therefore, the autocorrelation function is noisy and asymmetric (Fig. 6) and the reconstructed bunch shape (Fig. 7) less accurate. When electron bunches are at maximum compression, the intensity of the coherent transition radiation is high and the autocorrelation function is less noisy and symmetric (Fig. 4).

In order to obtain a good approximation of the form factor phase, the upper limit of the integral in Eq. (3) is set at 5 THz, which is well beyond the frequency where data is available. The asymptotic expression at high frequencies (Fig. 6 bottom plot) is used to evaluate intensity in this spectrum domain.

The intensity spectrum-completion procedure is plagued by uncertainties, because it is not obvious what "low and high frequencies" really means, and interpolation procedures are somewhat arbitrary.

Since the sensitivity of Golay detectors is reasonably good at low frequencies (down to 10 GHz), the intensity spectrum needs to be completed with only a few points. For the case shown in Fig. 6, the parameters a and b from Eq. (10) were determined from a least-squares fit with five data points corresponding to frequencies below $0.5\omega_0 \approx 0.1$ THz. The longitudinal charge distribution is only slightly affected by the number of data points taken into account to evaluate the parameters from Eq. (10).

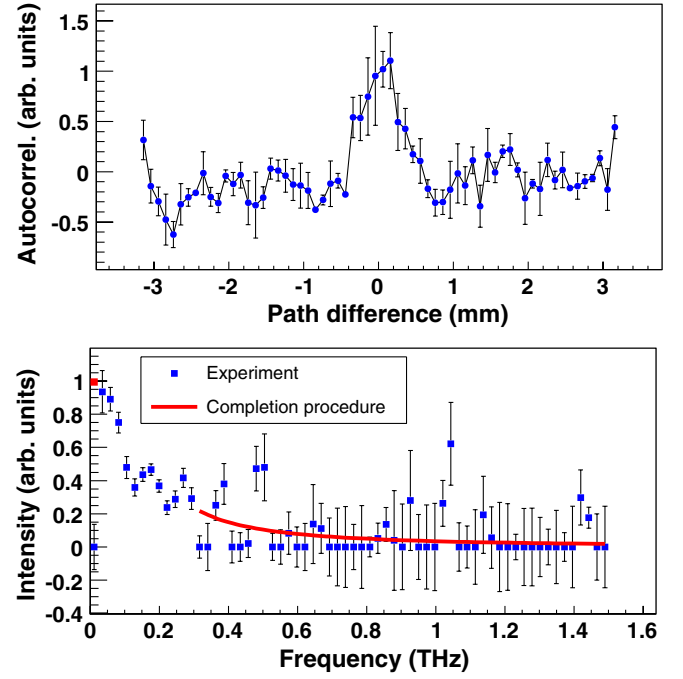


FIG. 6. (Color) Autocorrelation function (top) and completed intensity spectrum (bottom) for 3.2 nC electron bunches at moderate compression. The solid curve (bottom) is the asymptotic intensity spectrum at high frequencies. Data points with negative values of the intensity were set to zero. The unknown parameters from Eq. (11) were determined from a least-squares fit with data points corresponding to frequencies higher than $2\omega_0$. A Golay detector was used for these measurements.

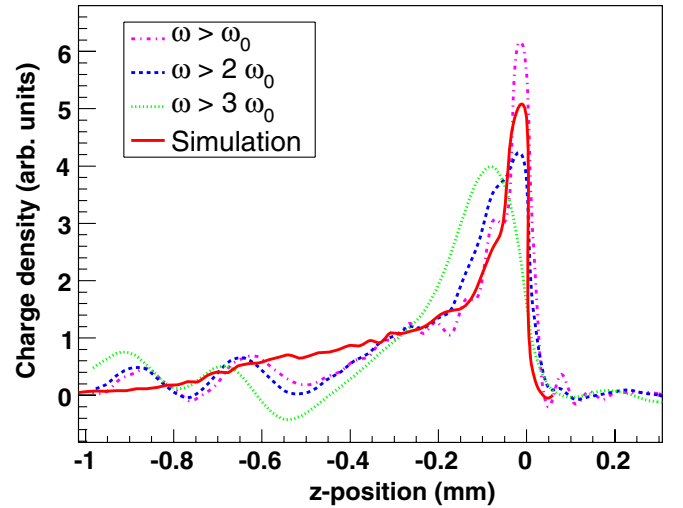


FIG. 7. (Color) Variations of the longitudinal charge distribution due to intensity spectrum-completion procedure at high frequencies. The intensity spectrum at large frequencies was completed by fitting the asymptotic power function with data points from different frequency ranges. The best agreement with simulations is achieved for $\omega > 2\omega_0$. Experimental and simulation results were obtained for 3.2 nC electron bunches at moderate compression.

Above 0.3 THz, the intensity spectrum contains several missing frequency regions. To estimate the uncertainties related to the intensity spectrum-completion procedure, the parameters in Eq. (11) were obtained by fitting with data points from different frequency domains. Figure 7 shows the variations of longitudinal charge distribution due to intensity spectrum completion at high and medium frequencies as well as a simulation result for 3.2 nC electron bunches at moderate compression. In general the agreement between measurement and simulation is within 30% for bunch length and peak height. For the case shown in Fig. 7 the measured bunch length is 0.97 ps (when the intensity spectrum was completed by fitting data points with $\omega > 2\omega_0$) and the simulated bunch length is 0.83 ps.

As a general rule, the inaccuracies in spectrum completion at low frequencies are critical for relatively long electron bunches (picosecond range), because the intensity spectrum in this case is predominantly located in the low-frequency region (below 0.2 THz). Similarly, the shape of short electron bunches (like those used for FEL) will mostly be affected by spectrum completion at high frequencies.

High charge density at the head of the electron bunch is due to nonlinear effects in the bunch compression. The width of the peak, as well as the shape and the length of the charge distribution tail, can be related to energy spread, nonlinearity of the rf field, and to bunch compressor parameters R_{56} and T_{566} [22].

C. Complicated longitudinal shapes

Longitudinal distribution of the electron bunches at the cathode is determined by the temporal structure of the laser beam. Under normal operation conditions at the Fermilab/NICADD photoinjector, the laser pulses have an approximate Gaussian shape with a typical duration of about 2.4 ps (rms). For beam physics studies the laser system was modified to produce up to 4 pulses separated by an adjustable time delay. This feature of the laser system was also used to test how well our interferometric method works when electron bunches have a more complex longitudinal shape.

At the Fermilab/NICADD photoinjector, double-peaked non-Gaussian pulses were used for direct measurements of the momentum compaction of the magnetic bunch compressor [15]. Longitudinal diagnostics based on coherent transition radiation is useful to determine the separation and the shapes of the two pulses after compression.

Electron bunches consisting of two sub-bunches were generated with a temporal separation of 15 ps prior to the bunch compression. The charge of each pulse was about 0.5 nC. Experimental conditions can be set such that maximal compression occurs at any distance from the leading pulse. Assuming that one of the two pulses is maximally compressed, the autocorrelation and the reconstructed bunch shape would be similar to those of single

pulse bunches. The reason is that the pulse which is less compressed is too wide to produce enough coherent radiation. Also, if maximum compression is set at the mid-distance from the two pulses, they overlap during compression and, again, no sign of double-peaked bunch can be observed. In order to be able to measure more complicated longitudinal charge distributions, maximum compression should occur between the two pulses and closer to one of them.

Figure 8 shows the autocorrelation function, reconstructed and simulated longitudinal shape, when the temporal distance between pulses is 15 ps and the maximum compression was set at 6 ps from the first pulse. Since neither of the two pulses is at maximum compression, the intensity of the coherent radiation is low and correlation function is noisy and a little asymmetric.

The agreement between experiment and simulation is still good although not as good as in the case of single pulse bunches. This happens because the expression for the form factor phase [Eq. (3)] is a less accurate approximation when the bunch structure is more complicated. It was shown [23] that bunches with two components can still be reconstructed correctly if the larger component comes first (as in the case depicted in Fig. 8). When the smaller component comes first, the reconstructed longitudinal bunch shape is significantly distorted, but still the calculated widths are correct.

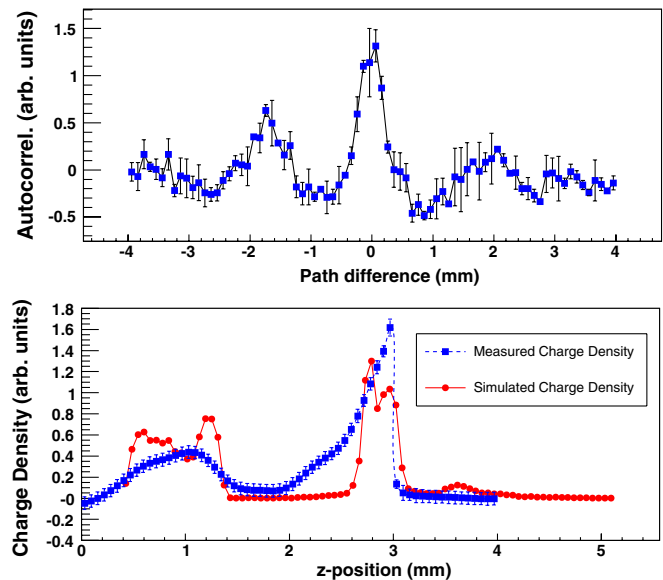


FIG. 8. (Color) Autocorrelation function (top) for electron bunches consisting of two pulses separated by 15 ps before the bunch compression. Each pulse had about 0.5 nC. Maximum compression was set to occur at a position located between the two pulses and closer to the leading one. Longitudinal charge distributions from experiment (red line) and simulation (blue line) are shown in the bottom plot. For these settings of the photoinjector, the overall compression factor is about 2.5.

V. CONCLUSIONS

We performed measurements of longitudinal charge-density profiles for electron bunches consisting of either one or two Gaussian-shaped pulses before being compressed. Agreement with simulation is quite good. There are two major sources of systematic uncertainties in this analysis: (1) the inaccuracy of the interferometer's response function, and (2) the ambiguities of the intensity spectrum-completion procedure. We combatted the former by inferring the response function with the aid of simulation. We used both pyroelectric and Golay detectors, and concluded that Golay detectors are better suited for this kind of measurement because their response is more uniform over a larger spectral range.

The limitations of the interferometric method are mainly due to low detector sensitivity and diffraction at low frequencies, and to absorption in optical components at high frequencies. Also, since the instrument is sensitive only to transition radiation with a certain degree of coherence, only bunches shorter than about 2 ps can be measured. In turn, one can resolve localized (~ 2 ps) prominent features over a long (~ 10 ps) density profile (cf. Fig. 8).

ACKNOWLEDGMENTS

We would like to thank J. Li and R. Tikhoplav for their support with laser-related activities. This work was supported by DOE Grant No. DE-FG02-04ER41323 and Air Force Contract No. FA9471-040C-0199.

[1] V. Avyazian *et al.*, Eur. Phys. J. D **20**, 149 (2002).

- [2] Tesla XFEL Technical Design Report, Desy 2002-167, 2002.
- [3] U. Happek *et al.*, Phys. Rev. Lett. **67**, 2962 (1991).
- [4] Y. Shibata *et al.*, Phys. Rev. A **45**, R8340 (1992).
- [5] J.S. Nodvick and D.S. Saxon, Phys. Rev. **96**, 180 (1954).
- [6] C.J. Hirschmugl *et al.*, Phys. Rev. A **44**, 1316 (1991).
- [7] R. Lai and A.J. Sievers, Nucl. Instrum. Methods Phys. Res., Sect. A **397**, 221 (1997).
- [8] Fermilab/NICADD website: <http://nicadd.niu.edu/fnpl>.
- [9] R. Lai, U. Happek, and A.J. Sievers, Phys. Rev. E **50**, R4294 (1994).
- [10] S. Zhang *et al.*, JLAB-TN-04-024, 2004.
- [11] A. Murokh *et al.*, Nucl. Instrum. Methods Phys. Res., Sect. A **410**, 452 (1998).
- [12] M. Geitz *et al.*, Proceedings of the 1999 Particle Accelerator Conference, New York, 1999, p. 2172.
- [13] Information about pyroelectric detector (model P4-45) can be found on Coherent Inc. website: <http://www.coherent.com/>.
- [14] M.J.E. Golay, Rev. Sci. Instrum. **18**, 347 (1947).
- [15] P. Piot *et al.*, Phys. Rev. ST Accel. Beams **9**, 053501 (2006).
- [16] L. Young, LANL Report No. LA-UR-96-1835.
- [17] J. Qiang *et al.*, Proceedings of 2005 IEEE Particle Accelerator Conference (PAC 05), Knoxville TN, 2005), p. 3316.
- [18] M. A. Geitz, DESY-THESIS-1999-033, p. 99.
- [19] C. Settakorn *et al.*, SLAC PUB 7586, 1-4, 1997.
- [20] H. Loos (private communication).
- [21] M. Castellano *et al.*, Proceedings of 1999 Particle Accelerator Conference, New York, NY, 1999, p. 2193.
- [22] R. Li, Nucl. Instrum. Methods Phys. Res., Sect. A **475**, 498 (2001).
- [23] R. Lai and A. J. Sievers, Phys. Rev. E **52**, 4576 (1995).